Proc. Natl. Conf. Theor. Phys. **35** (2010), pp. 92-100

DENSITY FUNCTIONAL BASED TIGHT BINDING STUDY ON WURZITE CORE-SHELL NANOWIRES HETEROSTRUCTURES ZnO/ZnS

N.T. THUONG[1], N.V. MINH[1], N.N. TUAN[1] and V.N. TUOC [1,2,3]
[1]*Institute of Engineering Physics (IEP), Hanoi University of Science and Technology (HUST), 01 Dai Co Viet Str., Hanoi 10000, Vietnam*
[2] *International Center for Computational Materials Science (ICCMS), Hanoi University of Science and Technology (HUST), 01 Dai Co Viet Str., Hanoi 10000, Vietnam*
[3]*Department of Materials Science and Engineering, Univ. of Illinois at Urbana Champaign, USA*

Abstract. *We present a Density Functional Based Tight Binding study on the crystallography and electronic structures of various II-VI wurtzite core-shell, core-multi-shell ZnO/ZnS unsaturated nanowires (NW) of circular and hexagonal cross sections and examine the dependence of interface stress and formation energy on nanowire lateral size with diameter range from 20Å upto 40Å. Young's modulus of the wires along the axial growth direction have been estimated. Also the tensile test have been applied for various wires to show the diameter dependences of their mechanical properties. The electronic properties of these heterostructure nanowires (e.g., Projected Band Structure, Density of State, charge transfer via Mulliken population analysis) also exhibit diameter-dependent behavior.*
PACS: 31.15.E-, 61.46.Km, 61.46.Np, 71.15.-m, 73.20.-r
Keyword: Wurtzite Nanowire, Density functional based tight binding simulation

I. INTRODUCTION

Nanostructured ZnO materials have been the subject of intensive study owing to their distinguished performance in optoelectronics, sensors, transducers, and biomedical sciences. ZnO materials have three key properties: (i) direct-wide bandgap (3.37eV ∼375nm at 300K), polar surface, high exciton binding energy (60 meV) which may result in high efficient light emitting nano device (blue LED, nanoscale UV laser, photo-detector). Its transparent conductivity may find application in flat panel display, solar cell, (ii) the lack of a centre of symmetry in wurtzite, combined with its large electromechanical coupling, resulting in strong piezoelectric and pyroelectric properties and the consequent use of ZnO in surface acoustic wave device for communication and sensing applications, (iii) its biosafety and biocompatibility may result in many biomedical applications without coating. When doped with transition metals, it can form spin-polarized light sources and could be diluted magnetic semiconductor. In addition, ZnO nanowire can be synthesized using diverse techniques and its ability to manipulate and align these individual nanostructures is necessary for wafer-based large scale integration.

Nanowire (NW) is quasi-one dimension (1D) single crystalline, dislocation free, with atomically flat surfaces, which is interesting as material for future's nanofunctional devices of key importance, e.g., FET (Field-effect transistors), gas sensors, nano-resonators, nano-cantilever, bio-sensor.

ZnO nanowires usually grow along the [0001] direction and have the same structure as their bulk wurtzite phase [1, 2]. For sufficiently thin ZnO nanowire, quantum size effects are expected to have a dominant influence, e.g., significant enhancement of the exciton binding energy in the colloidal-synthesized ZnO nanowire with average diameter of 2.2 nm and average length of 43 nm was observed, which implies a promising candidate for ultraviolet laser devices operating at room temperature [1]. Since ultra thin ZnO nanowires are single crystalline and nearly defect-free, their high surface-to-volume ratios enhance atomic mobility and promote structural reconstruction. Different from the nanotubes, whose electronic properties are largely determined by the chirality of the nanotubes, nanowires have the advantage that many of their properties, particularly electronic structure, can be controlled during growth by varying the size, composition, and growth direction [2].

Integrated circuit conventional down scaling while maintaining devices basic structure faced now fundamental challenges - integrate novel 1D structures: Carbon Nano Tube (CNT) and NW. Very recently, Wang has reported the mass production of single crystalline NW and nanocables ZnO/ZnS via a thermal reduction route by graphite powder.

One major motive is the solar cell nanowire. The production of silicon-based photovoltaics are now limited by the high cost and energy input required to create the highly purified silicon. Alternative approaches, such as thin-film devices, based either on toxic and less abundant CdTe and CdSe, and organic photo-voltaics suffer from low efficiency and short operating lifetimes, respectively. Therefore, the oxide-based semi-conductor materials are attractive due to their abundance, chemical stability, and lack of toxicity. ZnO is widely known as a paint pigment and as a sunscreen. Besides merely using the bulk, one may also consider whether quantum size effects may be useful. Unfortunately, due to the reason of high band gap, it is too large for use ZnO in efficient photo-voltaic devices. Nonetheless, this has not prevented numerous attempts to construct photovoltaics from this material, with schemes such as compound thin film heterojunctions, e.g., ZnO/CdSe, n-ZnO/p-Si or composites heterostructures [3]. Further approach is to reduce the band gap of ZnO is to stack it with another environmentally benign and abundant material, such as ZnS. Because of the staggered type-II band alignment, the band gap of the composite structure could be much smaller than either of the individual materials. Various efficient experimental techniques have been applied for the partial conversion of ZnO nanowires into ZnO/ZnS core/shell nanowires (see [4] and references there in). Zinc-containing systems have been widely investigated by first-principles methods [5, 6, 7, 8]. However, it becomes difficult to treat a large number of atoms because of their high computational demands. Therefore, self-consistent charge density-functional tight-binding (SCC-DFTB) method [9, 10, 11], which has been successfully applied to large-scale quantum-mechanical

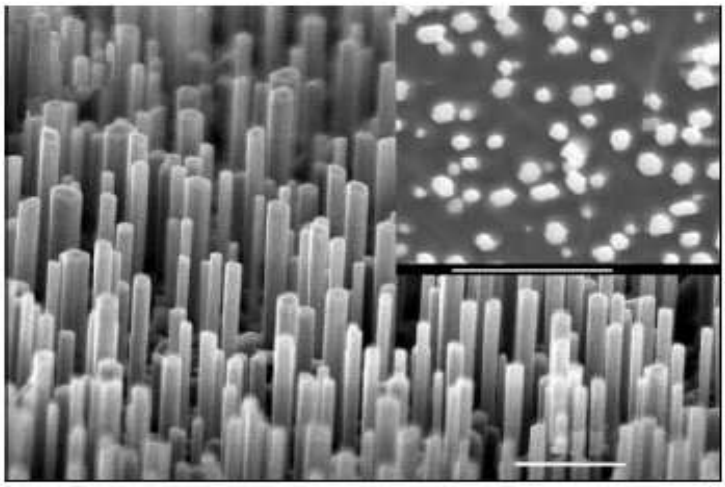

Fig. 1. NW taken from NANOSTRUCTURES IN ELECTRONICS AND PHOTONICS, Faiz Rahman 2008.

simulations, is suitable candidate for the task. The method is an approximation to the Kohn-Sham density-functional theory (DFT), which combines reasonable accuracy and computational efficiency. The present work represents an extensive study of ZnO/ZnS hetero wurtzite systems, which we perform using first-principles Density Functional Tight-Binding calculations.

II. DENSITY-FUNCTIONAL-BASED TIGHT-BINDING PLUS (DFTB+) METHOD

The spin-polarized, charge self-consistent, DFTB approach is based on a second-order expansion of the spin-dependent Kohn-Sham total energy functional with respect to a given reference charge and magnetization density. The method has been extensively discussed elsewhere [9, 10, 11, 12] and briefly outlined here as:

1/ Expand the orbitals as a linear combination of Slater type orbitals (LCSTO):

$$\psi_n(r) = \sum_{\text{atomic site } i} \sum_{\text{orbital } \nu} C_{i\nu}\phi_{i\nu}(\mathbf{r} - \mathbf{R}_i) \tag{1}$$

The basis functions $\phi_{i\alpha}(\mathbf{r} - \mathbf{R}_i)$ centered on the atomic nucleus i, with position $\mathbf{R}_i$, are themselves a linear combination of single Slater orbitals $\phi_\nu(\mathbf{r}) = (\sum_{j=1}(\sum_{n=0} a_{jn}\mathbf{r}^{l_\nu+n})e^{-\alpha_j r})Y_{l_\nu m_\nu}$. The angular and magnetic quantum number are indicated with l_ν and m_ν. $Y_{l_\nu m_\nu}$ is the corresponding real spherical harmonic.

2/ Tight-binding expansion of the wave functions (calculation of the matrix elements in the two-center approximation).

$$\sum_{\text{atomic site } i} \sum_{\text{orbital } \nu} |H_{i\nu,j\mu} - ES_{i\nu,j\mu}| \, C_{i\nu,j\mu} = 0 \tag{2}$$

with

$$H_{i\nu,j\mu} = \left\langle \phi_{i\,\nu} | \hat{H} | \phi_{j\,\mu} \right\rangle \tag{3}$$

and

$$S_{i\nu,j\mu} = \langle \phi_{i\,\nu} | \phi_{j\,\mu} \rangle \tag{4}$$

3/ Second order-expansion of Kohn-Sham energy functional (self-consistency in the charge density - SCC-DFTB):

$$E_{tot} = \sum_{i}^{occ.} n_i \langle \psi_i | \, H_0 \, | \psi_i \rangle + \frac{1}{2} \sum_{\mu,\nu} \gamma_{\mu\nu} \Delta q_\mu \Delta q_\nu + E^{rep} \tag{5}$$

Where Δq_μ - charge fluctuation decomposed into atomic contribution (Mulliken charge), $\gamma_{\mu\nu}$ - some integral coefficient, E^{rep} - repulsive term (see Ref. 6-8). With all matrix

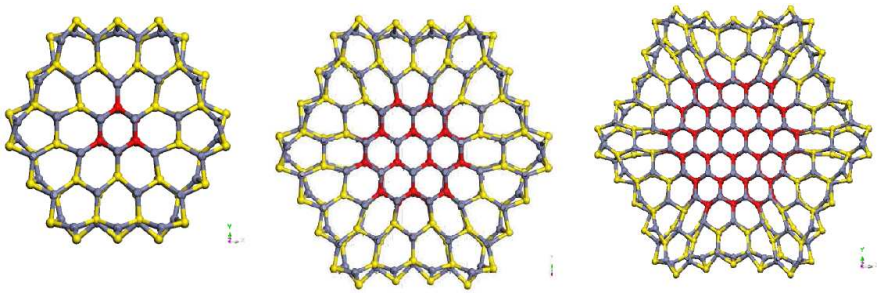

Fig. 2. Core-shell ZnO/ZnS heterostructure NW Nanowires in [0001] direction with fully optimized structures in cross section view.

elements and orbitals are derived from Density Functional calculation, the advantage of DFTB method relies on the use of small basic set of atomic orbitals (in order to reduce the matrix dimension for diagonalization speed-up) and the restriction to two center non-orthogonal Hamiltonian (allowing extensive use of look-up table). What it distinguishes from semi-empirical method is the explicit calculation of the basic wave function which allow deeper physics insight and better control of the approximation used. The method solved Kohn-Sham equation self-consistently using Mulliken charge projection. This approach have proved to give transferable and accurate interaction potential, as well as numerical efficiency allowing Molecular Dynamic (MD) simulation of super-cell containing about hundred to thousand atoms. Thus, this is particular suitable to study the electronic properties and dynamics of large mesoscopic system and organic molecule such as CNTs, DNA stands or absorbs on surface, semiconductor hetero-structure, etc., see review in Ref. 4-6. The advantage of DFTB parameterization is that only few, possibly well chosen systems are needed to create the parameters, i.e., in DFTB fit systems can also be purely

ideal systems, if they are chemically acceptable and can be described carefully with an ab-initio approach. Next this well tested parameter, e.g., in an attention for solid state systems and for defect physics as in current case, can be used for much larger system due to its transferability. In our calculation the parameter and its transferability have been successfully applied in several DFTB works [13, 14, 15, 16].

The electronic DFTB parameters (i.e., Hubbard parameters, ν and $S_{\mu\nu}$ matrix elements) were derived directly from DFT calculations, performed within the generalized gradient approximation (GGA) and using the Perdew, Burke, and Ernzerhof (PBE) exchange-correlation functional.

III. RESULTS AND DISCUSSION

III.1. Atomic structure

Two type of the hereto-structures (HS) are created for simulation purpose: (i) hetero-structure core-shell ZnO/ZnS coaxial nanowire, (ii) core-multishell ZnO/ZnS/ZnO or coaxial quantum well.

Fig. 2 shows the three representatives of the Core-shell ZnO/ZnS heterostructure NW Nanowires in [0001] direction with fully optimized structures in cross section view with description in Table 1:

Table 1. Stoichiometry of ZnO/ZnS heterostructure.

$Core-shell\ (from\ left\ to\ right)$	1	2	3
$Diameter\ (A)$	19.5	26.9	34.6
$Total\ number\ of\ atom\ in\ supercell$	108	192	300
$Highest\ Occupied\ Molecular\ Orbital\ (HOMO)\ level$	486	864	1350
$Total\ number\ of\ Atomic\ Orbitals\ (AO)\ used$	702	1248	1950

$Core-shell\ (from\ left\ to\ right)$	1	2
$Diameter\ (A)$	37.9	39.6
$Total\ number\ of\ atom\ in\ supercell$	300	432
$Highest\ Occupied\ Molecular\ Orbital\ (HOMO)\ level$	1350	1944
$Total\ number\ of\ Atomic\ Orbitals\ (AO)\ used$	1950	2808

Similar to our recent work on pure ZnO nanowire, we examine the nanowires with different shapes, when dangling bonds are not saturated then the surface relaxation in a nanowire occurs inevitably compare to that is taken from its stress-free bulk wurtzite counterpart, which is stable phase for ZnO/S at 300K. This relaxation may initially deform the nanowire without any applied loads. Therefore, relaxation must be conducted in atomic simulations of nanowires to let them reach thermodynamics equilibrium state in both wire's growth direction [0001] (wire axial) and its perpendicular surface.

However, it should be noted that ZnO and ZnS are very similar material but one is very large lattice mismatch. The experimental bulk lattice parameter are for ZnO ($a = 3.25, c = 5.21$) vs. ZnS ($a = 3.81, c = 6.23$) which coresponding the mismatch

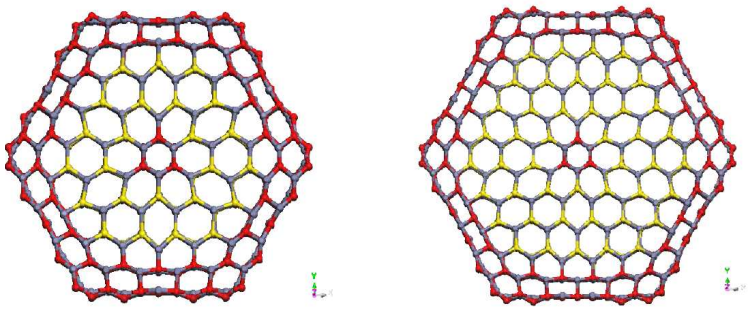

Fig. 3. Core-multi shell ZnO/S heterostructure NW in [0001] direction with fully optimized structures in cross section view.

as $c^{\mathrm{ZnS}}/c^{\mathrm{ZnO}} = 1.197\,(\sim 6/5)$ and $a^{\mathrm{ZnS}}/a^{\mathrm{ZnO}} = 1.17\,(\sim 7/6)$, i.e., their bulk plane heterostructure very closed to the Domain Match Epitaxy (DME) scheme [17], and which will result in the misfit dislocations right in the interface. So that we put here a simulation task to see how does this HS relax their strain in co-axial fashion as core-shell and core-multishell structures? Does ZnO can host ZnS without a dislocation at the interface? From the relaxed structure analysis we may come to the conclusion as: (i) at outer layer, Zn (anion site) move inward - shrinking distance to neareast Zn, the O or S atom site approximately remain unchanged, (ii) hetero bond of Zn-O/S bondlength at surface/interface have been constricted (5.4%-4.7%) and (2.5%-1.2%), (iii) inner layer's change is less than ∼0.3-0.5%. Two atomic layer beneath the interface stay nearly unchanged. This behavior is found across the entire range of diameters of nanowires examined, (iv) in the free relaxed wires with c is lattice parameters along wire direction, the HS wires also are strained toward the manner of stretched the core part (since bulk lattice of ZnO is smaller than the ZnS) whereas ZnS is compressd. Fig. 4 shows the depences of this wire's relaxed c-axis on wire's diameter of different HS wires, which show a competition tendency between stretch from ZnO side and compress from ZnS, depend on their composition content.

III.2. Heterostructure wire band structure

Band structures for relaxed HS nanowires are shown in Fig. 5 along the $\Gamma - Z$ direction (parallel to wire direction see inset scheme in Fig. 6). The 1D band structures were computed using $1\times1\times20k-$point set. Similar to result of our previous [18], the band gap decreases with increasing nanowire diameter approaching bulk parameter. The band analysis show that the top of valence band does not change much for all the wires, but the bottom of the conduction band moves up as the diameter decreases, which results in the band gap becoming wider. Also for all HS wires, the bottom of conduction band and the top of valence band were both located in Γ point of the Brillouin zone, indicating a direct band gap semiconductor. The red-like in the first bandstructure shows the quadratic fitting line to determine the effective mass of electron (at the bottom of conduction band) and of hole (at the top of valence band) using expression $\Delta E_{c/v}(\mathrm{k}) = \pm\hbar^2\mathrm{k}^2/2m^*_{e/h}$. We expected that change in band structure and gap with diameter lead to the change in effective mass

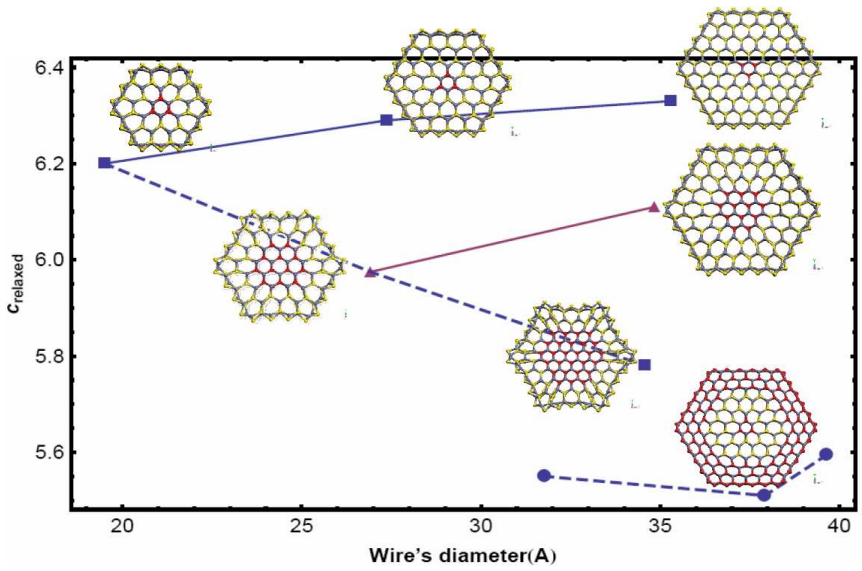

Fig. 4. Relaxed lattice parameters of HS NW along [001] vs wire's diameter.

of electron and hole in NW growth direction. The effective mass of the electron is smaller than those in the bulk value so this may produce higher electron mobility but not in the case of hole mobilities.

III.3. Core/shell nanowire for solar cells.

Fig. 6 shows that while stacking two such large band gap materials (ZnO and ZnS) together, they are forming a hetero junction with type-II band alignment - which means one material's Valence Band Maximum (VBM) and Conduction Band Maximum (CBM) are both higher than the other materials' VBM and CBM, respectively. Therefore, the overall band gap that count from the lower CBM to higher VBM of the whole system will be reduced, thereby making its gap suitable for solar cell, i.e., ∼2eV. This small combined gap occurs only near the interface, it is necessary to make such a device in nanoscale, so that interface area occupies a big proportion of system (or high surface/volume ratio as NW). Moreover, in HS nanowire with radial junctions the e-h separation can occur on very short spatial scales, and thus recombination can be suppressed more effectively. Therefore HS nanowire simultaneously perform all four key functions of the ideal solar cell: (i) light harvesting due to their high surface/volume ratio, i.e., lateral radial nanoscale, (ii) energy conversion - ability to tune the bandgap by varying the diameter of HS content, i.e., alignment and size dependent quantum effect, (iii) charge separation, since the HS is type II HS so that combined gap occurs in very small area, and (iv) charge transport due to lateral nano size of HS core-shell/multishell and the reduction effective mass of electron/hole.

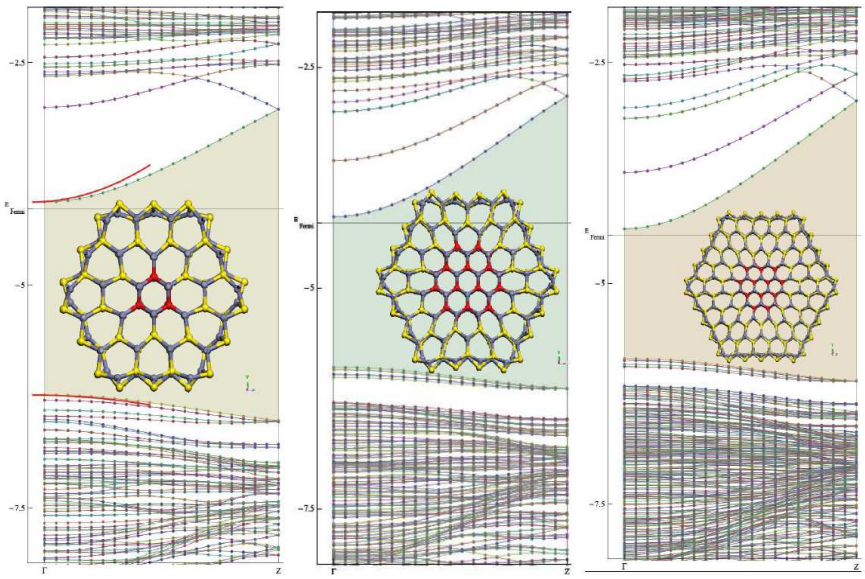

Fig. 5. The band structures for some representative relaxed HS nanowire.

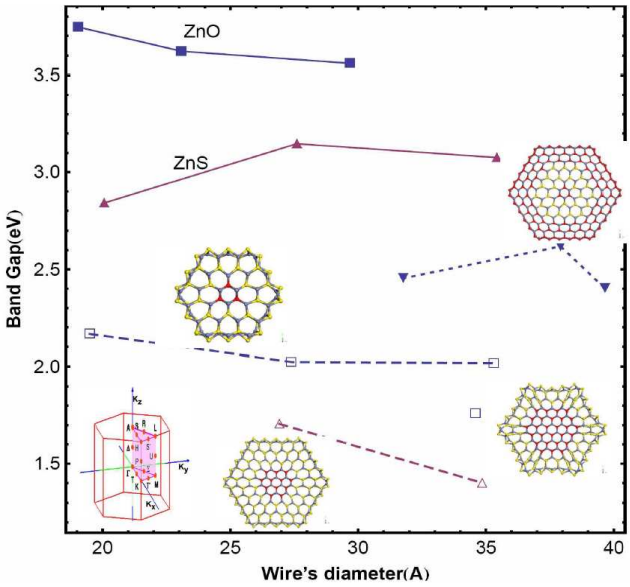

Fig. 6. Band gap HS NW along [001] vs wire's diameter.

IV. CONCLUSIONS

Calculations presented in this work demonstrate that the formation of ZnO/ZnS nanoheterostructures can substantially reduce the optical band gap while simultaneously maintaining required optical absorption. The geometry and size dependence of relaxed core-shell and core-multishell NW morphology shows the shrinkage of outermost layer at anion site but not at the interface which is quite like in homogenious structure, i.e., no defect formation, together with the elongation/compress different HS nanowire content along growth direction. It also shows that the radial quantum well (QW) can be created along HS NW and for ZnO/ZnS whereas plane QW can not be due to its larger mismatch. Electronic properties including bandstructure, effective mass are also found to depend on NW lateral parameters.

ACKNOWLEDGMENT

This work was supported by the Vietnamese Project QG TD 09-05

REFERENCES

[1] M. Yin, Y. Gu, I. L. Kuskovsky, T. Andelman, Y. M. Zhu, G. F. Neumark, S. O'Brien, *J. Am. Chem. Soc.* **126** (2004) 6206.
[2] Matt Law, Joshua Goldberger, Peidong Yang, *Semiconductor Nanowires and Nanotube, Annual Review of Materials Research* **34** (2004) 83-122.
[3] G. Wary, T. Kachary, A. Rahman, *Int. J. Thermophys.* **27** (2006) 332.
[4] S. Panda, A. Dev, S. Chaudhuri, *J. Phys. Chem. C* **111** (2007) 5039.
[5] B. Wang, J. Zhao, J. Jia, D. Shi, J. Wan, G. Wang, H. Xu, *Appl. Phys. Lett.* **93** (2008) 021918.
[6] Guofeng Wang, Xiaodong Li, *Appl. Phys. Lett* **91** (2007) 231912.
[7] Y. Maoa, J. Zhonga, Y. Chen, *Physica E* **40** (2008) 499-502.
[8] Y.R. Yang, X.H. Yan, Y. Xiao, Z.H. Guo, *Chem. Phys. Lett.* **446** (2007) 98-102.
[9] M. Elstner, D. Porezag, G. Jungnickel, J. Elsner, M. Haugk, Th. Frauenheim, S. Suhai, G. Deifert, *Phys. Rev. B* **58** (1998) 7260.
[10] C. Kohler, G. Seifert, Th. Frauenheim, *Chem. Phys.* **309** (2005) 23.
[11] M. Elstner, D. Porezag, G. Jungnickel, J. Elsner, M. Haugk, T.; B. Aradi, B. Hourahine, Th. Frauenheim, *J. Phys. Chem. A* **111** (2007) 5678.
[12] B. Aradi, B. Hourahine, Th. Frauenheim, *J. Phys. Chem. A* **111** (2007) 5678-5684.
[13] Ney H. Moreira, Grygoriy Dolgonos, Ba'lint Aradi, Andreia L. da Rosa, Thomas Frauenheim, *J. Chem. Theory Comput.* **5** (2009) 605-614.
[14] R.Q. Zhang, X. Zhang, A.L. Rosa, Th. Frauenheim, *Nanotechnology* **18** (2007) 485713.
[15] W. Fan , H. Xu, A. L. Rosa, Th. Frauenheim, R. Q. Zhang, *Phys. Rev. B* **76** (2007) 73302.
[16] H. Xu, A. L. Rosa, Th. Frauenheim, R. Q. Zhang, S. T. Lee, *Applied Phys. Lett.* **91** (2007) 31914.
[17] V.N. Tuoc, *Mat. Transactions* **49** No.11 (2008) 2491-2496.
[18] V.N. Tuoc, *Comp. Mat.Sci.* **49** No.4 (2010) 161-169.

Received 10-10-2010.